Toxicology Letters 289 (2018) 1–13

Contents lists available at ScienceDirect

Toxicology Letters

journal homepage: www.elsevier.com/locate/toxlet

Integrated 'omics analysis reveals new drug-induced mitochondrial perturbations in human hepatocytes

Jarno E.J. Wolters[a,*], Simone G.J. van Breda[a], Jonas Grossmann[b], Claudia Fortes[b], Florian Caiment[a], Jos C.S. Kleinjans[a]

[a] Department of Toxicogenomics, GROW-School for Oncology and Developmental Biology, Maastricht University Medical Center, P.O. Box 616, 6200 MD Maastricht, The Netherlands
[b] Functional Genomics Center Zurich, Functional Genomics Center Zurich, University Zurich/ETH Zurich, Winterthurerstrasse 190, 8057 Zurich, Switzerland

ARTICLE INFO

Keywords:
Steatosis
Mitochondrial dysfunction
Primary human hepatocytes
Epigenomics
Transcriptomics
Proteomics

ABSTRACT

We performed a multiple 'omics study by integrating data on epigenomic, transcriptomic, and proteomic perturbations associated with mitochondrial dysfunction in primary human hepatocytes caused by the liver toxicant valproic acid (VPA), to deeper understand downstream events following epigenetic alterations in the mitochondrial genome. Furthermore, we investigated persistence of cross-omics changes after terminating drug treatment. Upon transient methylation changes of mitochondrial genes during VPA-treatment, increasing complexities of gene-interaction networks across time were demonstrated, which normalized during washout. Furthermore, co-expression between genes and their corresponding proteins increased across time. Additionally, in relation to persistently decreased ATP production, we observed decreased expression of mitochondrial complex I and III–V genes. Persistent transcripts and proteins were related to citric acid cycle and β-oxidation. In particular, we identified a potential novel mitochondrial-nuclear signaling axis, MT-CO2–FN1–MYC–CPT1. In summary, this cross-omics study revealed dynamic responses of the mitochondrial epigenome to an impulse toxicant challenge resulting in persistent mitochondrial dysfunctioning. Moreover, this approach allowed for discriminating between the toxic effect of VPA and adaptation.

1. Introduction

Unforeseen liver injury is a major cause of drug failure during clinical trials and upon market introduction. It is therefore widely held that improved biomarkers for drug safety, derived from deeper mechanistic insights in drug-induced molecular perturbations of the human genome and applicable in the (pre-) clinical phase, are needed for better predictions of drug safety. Cross-omics analysis of toxic events in relevant human liver models, in full consideration of the dynamic features of biological systems by investigating the myriad of components of systems at multiple scales of cellular regulation, may deliver deeper knowledge of complex molecular mechanisms underlying drug-induced liver injury, and thus identify better biomarkers for drug safety. However, how to integrate temporal data from multiple 'omics analyses, with the purpose of capturing impulse responses of the methylome, the transcriptome, and the proteome to a particular toxic entity and in association with downstream functional parameters, still poses a substantial challenge to systems biology. Within this context we have developed a prototypical study on multiple 'omics integration across time in primary human hepatocytes (PHHs) treated with an established liver toxicant.

Steatosis is a subtype of drug-induced liver injury that refers to the process of abnormal retention of lipids within hepatocytes (Vinken, 2015). Steatotic compounds span a variety of therapeutic classes and their ability to cause adverse lipid accumulation is largely due to off-target effects which induce mitochondrial damage, in particular the inhibition of fatty acid β-oxidation, oxidative phosphorylation, and mitochondrial respiration (Schumacher and Guo, 2015).

B-oxidation is one of the primary routes through which lipids are metabolized, while the inhibition of β-oxidation leads to lipid retention in hepatocytes. Lipid metabolism via β-oxidation creates acetyl-Coenzyme A (CoA), which is subsequently used in the tricarboxylic acid (TCA) cycle (Ponchaut et al., 1992; Schumacher and Guo, 2015; Silva et al., 2001). NADH dehydrogenases (complex I in the electron transport chain (ETC)) convert lipids into CoA while NAD+ has been produced by using NADH (Chan et al., 2005; Hargreaves et al., 2016). This

* Corresponding author.
E-mail addresses: j.wolters@maastrichtuniversity.nl (J.E.J. Wolters), s.vanbreda@maastrichtuniversity.nl (S.G.J. van Breda), jg@fgcz.ethz.ch (J. Grossmann), claudia.fortes@fgcz.uzh.ch (C. Fortes), florian.caiment@maastrichtuniversity.nl (F. Caiment), j.kleinjans@maastrichtuniversity.nl (J.C.S. Kleinjans).

https://doi.org/10.1016/j.toxlet.2018.02.026
Received 18 December 2017; Received in revised form 2 February 2018; Accepted 23 February 2018
Available online 06 March 2018
0378-4274/

ETC ultimately produces ATP via ATP-synthase (complex IV of the ETC, such as *MT-ATP6* and *MT-ATP8*) (Schumacher and Guo, 2015). Here, an important enzyme is carnitine palmitoyltransferase I (*CPT1*) which is affected by nearly all steatohepatitis-inducing drugs (Schumacher and Guo, 2015). This enzyme shuttles fatty acid-CoA into the mitochondria for subsequent β-oxidation and represents the rate limiting step in β-oxidation.

Valproic acid (VPA) is one of the most widely prescribed anti-epileptic drugs in the world. Despite its pharmacological importance, it may cause liver toxicity, in particular steatosis (Jafarian et al., 2013; Silva et al., 2008). VPA is a simple fatty acid that is almost entirely metabolized by the liver (Silva et al., 2008). It is hypothesized that VPA exposure induces hepatotoxicity via oxidative stress, presumably by mitochondrial dysfunction (Chang and Abbott 2006; Jafarian et al., 2013; Tong et al., 2005). In the cytosol of hepatocytes, VPA is conjugated to valproyl-CoA which competitively and non-competitively inhibits *CPT1* (Aires et al., 2010). In addition, cytochrome P450 enzymes (CYPs) (such as *CYP2C9*, *CYP2B6*, and *CYP2A6*) play a role in VPA metabolism (Kiang et al., 2006). This affects the β-oxidation activity since it is regulated by CPT1 activity (Adachi et al., 2007) as well as VPA metabolism inside and outside the mitochondria (Chang and Abbott, 2006; Schumacher and Guo, 2015; Silva et al., 2008).

Conflicting arguments have been raised with regard to the issue whether the mitochondrial genome can be methylated (Bacalini et al., 2017; Iacobazzi et al., 2013; Manev and Dzitoyeva, 2013). In general, Sarkar et al. (Sarkar et al., 2011) has demonstrated that histone deacetylase (HDAC) inhibitors such as VPA, regulate gene methylation to repress mRNA expression of for example DNA (cytosine-5-)-methyltransferase 1 (*DNMT1*). Interestingly, VPA has been reported to affect methylation patterns in the mitochondrial DNA (mtDNA) from mouse fibroblast 3T3-L1 cells (Chen et al., 2012). In addition, Dong et al. showed that VPA induces DNA hypomethylation in nuclear DNA (nDNA) extracts of adult mouse brains (Dong et al., 2010). Occurrence of VPA-induced methylation in mtDNA and nDNA was confirmed by us in a previous study on PHHs (Wolters et al., 2017). In the present study, we aimed to investigate how VPA-induced epigenomic modifications in PHHs match with downstream changes on the transcriptome and proteome level, as well as with functional read outs for mitochondrial activity. Through this integrative cross-omics approach, we have been able to evaluate the impact of transient perturbations on the complex landscape of interacting gene regulatory networks in the human liver cell.

In view of the dynamics of cross-omics interactions (Bar-Joseph et al., 2012; Hendrickx et al., 2017) we have investigated the molecular effects of VPA in PHHs at multiple treatment time-points, as well as after terminating VPA administration in line with a recently published study design (van Breda et al., 2017). This washout (WO) mimicking a patient on transient or intermittent drug treatment (Tiwari et al., 2017) allows for evaluating persistence or reversibility of drug-induced toxicity (Rieswijk et al., 2016; Wolters et al., 2016) and has so far not been subjected to a cross-omics analysis. In addition, for the purpose of phenotypically anchoring cross-omics results (Bugiak and Weber, 2010; Porreca et al., 2014), we have analyzed ATP-production as an apical endpoint of mitochondrial dysfunction. For integrative analysis of cross-omics interactions we initially applied pathway mapping approaches in order to identify network propagation across time, followed by a supervised analysis applying Ordinary Differential Equation (ODE) (Huang et al., 2017) on a predefined fatty acid pathway.

2. Materials and methods

2.1. Cell culture and treatment

Cryopreserved Primary Human Hepatocytes (PHHs, Invitrogen) of 3 individuals (Hu8119, Hu1591 and Hu1540) were thawed for 1 min at 37 °C in a water bath. Next, these PHHs were pooled in order to bypass inter-individual variability in susceptibility to toxicants and cultured in 24-well plates in a collagen sandwich, according to the supplier's protocol (Invitrogen). In brief, 3 vials (one per individual) were thawed in 50 mL CHRM medium (CHRM CM7000, Invitrogen) and centrifuged for 10 min at 100*g* at 4 °C. After removing the supernatant, the cell pellet was dissolved in CHPM medium (CHPM CM9000, Invitrogen), which contain FBS, at a concentration of 1.0*10^6 cells/mL. Pooled PHHs were cultured in collagen-precoated 24-well plates (Gibco) (density: 0.35*10^6 cells/well) and cells were attached to the wells in the incubator for 4 h at 37 °C. After the incubation, the debris was removed by shaking and washing the cells twice with William's medium E (WME CM6000, Invitrogen). Subsequently, cells were covered by 150 µL/well of 1.0 mg/mL collagen-mixture (containing 10*DMEM, 1.0 mg/mL Collagen type 1 (BD), 0.2 M NaOH and, MQ) and incubated at 37 °C for approximately 30 min until the collagen was fixed. After that, culture medium (WME + 20 mL Hepatocyte Supplement Pack (CM4000, Invitrogen) substituted with 1% penicillin/streptomycin (Gibco)) was added.

After 3 days, the PHHs were exposed to 15 mM of VPA (IC_0 at 24 h of VPA-treatment and IC_{05} at 48 h) or 1% EtOH (vehicle control) in culture medium for 1, 2, and 3 day(s) daily. This concentration was used in an earlier study and we demonstrated that this incubation concentration induces observable steatosis in PHHs (Wolters et al., 2017). Here, we confirm 77% cell viability after 3 days of daily VPA-treatment (Fig. 1). Culture medium was changed daily thereby administering a new dose of VPA or EtOH to the cells. After the exposure period of 1, 2, and 3 days, the PHHs were captured for DNA, RNA, and protein isolation (DNA and RNA were from the same wells). Another well with PHHs was continued to be cultured for 3 consecutive days without VPA-treatment (from now on called washout period (WO-period)); the culture medium was again changed every day. All experiments were performed as biological triplicates for DNA and RNA isolation, while the protein isolation was performed in fourfold.

2.2. DNA and RNA isolation

PHHs were lysed in 250 µL Trizol/well. 6 wells were combined for each sample (2.1*10^6 cells in 1.5 mL Trizol). Phase separation and RNA isolation was performed according to the Trizol LS Reagent protocol (Life Technologies). The total amount of RNA obtained was around 5.0 µg of RNA, the 260/280 ratio varied between 1.7-1.9, and the 260/230 ratio was higher than 1.5.

The first part of the DNA isolation, DNA precipitation, was performed according to the Trizol LS Reagent protocol (Life Technologies). After that, DNA wash and resuspension was performed with minor adjustments. In short, after DNA precipitation the DNA pellet was washed using 75% EtOH. The tubes with their pellet were incubated for 10 min at room temperature and were occasionally mixed by gentle inversion. Tubes were centrifuged for 5 min at 2000*g* at 4 °C. Medium was discarded and pellets were vacuum dried for 5 min. Pellet was dissolved in 200 µL of nuclease free water. Add 5 µL preheated (for 30 min at 37 °C) proteinase K of 20 mg/mL to the samples and incubate for 1 h on a shaking heating block at 55 °C. After incubation for 1 h at 55 °C, the proteinase K was inactivated at 80 °C. 200 µL of phenol-chloroform-isoamylalcohol (PCI; 25:24:1) (Sigma) was added and shaken manually for 5 min. After centrifugation, the upper phase was again treated with 200 µL PCI. The upper phase was precipitated using 20 µL of 3 M NaAc pH 5.6 and 500 µL of cold 100% ethanol. The DNA pellet was washed using cold 70% EtOH, dissolved in 50 µL of nuclease free water and quantified spectrophotometrically using the NanoDrop 1000 (Thermo Scientific, Waltham, MA). The total amount of DNA obtained was at least 2.5 µg of DNA, the 260/280 ratio varied between 1.61-1.67, and the 260/230 ratio was higher than 1.5. For each replicate, one of the DNA isolations failed and therefore only biological duplicates were present for MeDIP-seq.

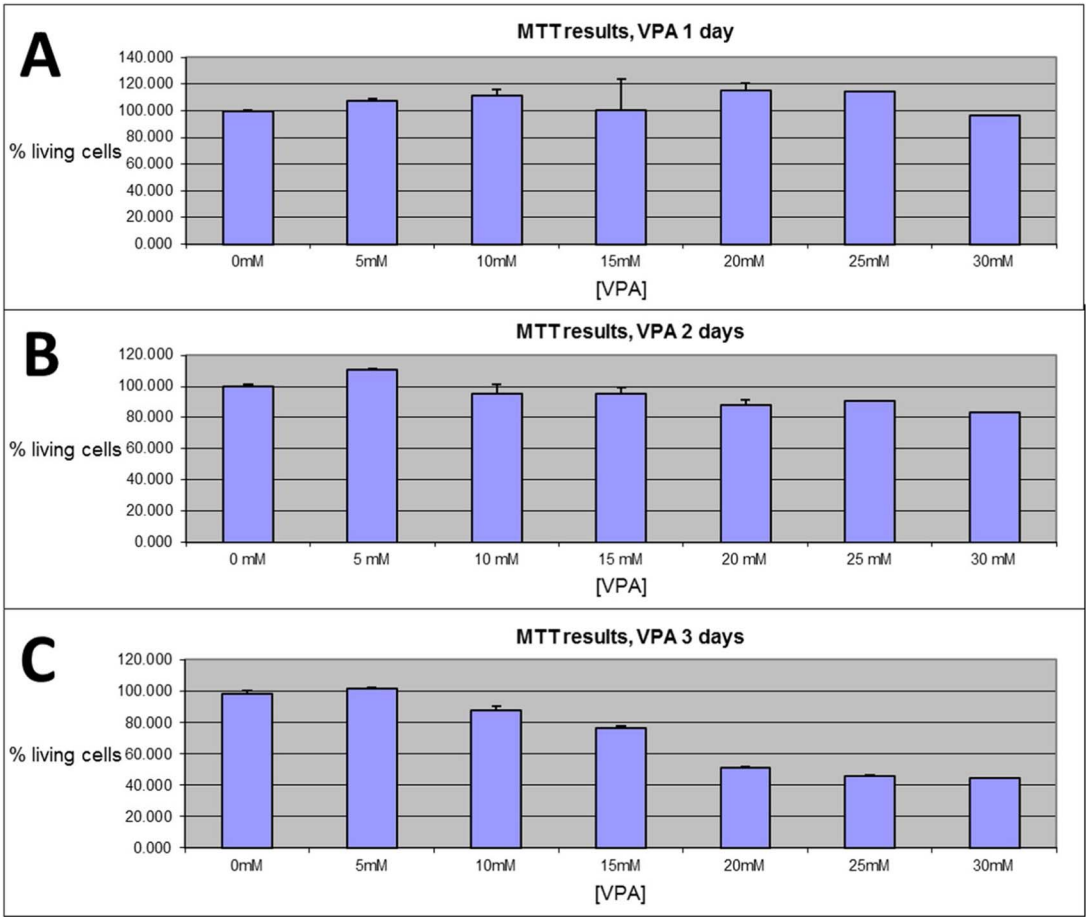

Fig. 1. MTT assay of PHHs exposed to a range of VPA concentrations (0, 5, 10, 15, 20, 25, and 30 mM) for 1 (A), 2 (B), and 3 (C) day(s) daily. PHHs, primary human hepatocytes; VPA, Valproic acid.

2.3. Protein isolation

PHHs were collected in 125 µL 1000U/mL collagenase KREBS buffer per well. 3 wells were combined for each sample (1.05*10^6 cells in 375 µL 1000U/mL collagenase KREBS buffer). In short, medium was discarded and cells were washed twice using PBS at room temperature. Thereafter, 125 µL pre-heated 1000U/mL collagenase KREBS buffer per well was added and incubated for 10 min at 37 °C. Add 1 mL of 1*PBS to each well, and thereafter the solution was resuspended and transferred into a 15 mL pointed Greiner tube. Repeat the previous step once. Tubes were centrifuged for 5 min at 65*g* at room temperature. Pellets were washed using 10 mL 1*PBS and centrifuged for 5 min at 65*g* at room temperature. This last step was repeated for all tubes and pellets were snap-frozen.

2.4. MeDIP-seq protocol

MeDIP-seq was performed according to the protocol of Taiwo et al. (Taiwo et al., 2012), with minor adjustments and has recently been published (Wolters et al., 2017).

The index primers (NEB) which were used as a barcode for each sample is reported in Supplementary Table S1. Furthermore, an overview of the sample location on the four separated channels of a 1.4 mm flow cell (Illumina) is shown in Supplementary Table S1. MeDIP-seq raw data are available on arrayExpress (accession number: E-MTAB-5983).

2.5. mRNA-seq protocol

mRNA quality was checked using the Agilent 2100 Bioanalyzer and RNA 6000 Nano chips (Agilent Technologies), according to the manufacturer's instructions. All RINs were higher than 9.30.

2.5.1. Library preparation

mRNA-seq library preparation was performed according to the manufacturer's instructions of the SENSE mRNA-Seq Library Prep Kit V2 for Illumina (Lexogen). Libraries were prepared using 500 ng of isolated RNA according to the manufacturer's protocol. PCR was used to amplify the mRNA fragments by using the included Barcode Sets 1–3 of the SENSE mRNA-Seq Library Prep Kit V2 for Illumina (Lexogen) (Supplementary Table S2).

DNA size and quality were checked using the Agilent 2100 Bioanalyzer and high-sensitivity DNA chips chips (Agilent Technologies), according to the manufacturer's instructions. Libraries were quantified on a Qubit fluorometer (Invitrogen) by using the Qubit RNA HS Assay kit (Invitrogen). All kits and chips were used according to the manufacturer's protocol.

2.5.2. Sequencing

The 24 amplified libraries (two times 12 samples), each sample having its own index primer, were pooled at an equimolar concentration of 2 nM, based on Qubit measurements. 20 pM of the 2 nM stock solution were then loaded onto four separated channels of a 1.4 mm flow cell (Illumina) (Supplementary Table S2) and cluster amplification was performed on a cBot (Illumina). Clustering, sequencing, base calling, de-multiplexing, and alignment was performed as described in

Wolters et al. (Wolters et al., 2017). mRNA-seq raw data are available on arrayExpress (accession number: E-MTAB-5984).

2.6. Protein protocol

2.6.1. Sample preparation

Extracted proteins were diluted 1:10 in SDS buffer (4% SDS, 100 mM Tris/HCL pH 8.2, 0.1 M DTT − dithiothreitol) boiled at 95 °C for 5 min and processed with High Intensity Focused Ultrasound (HIFU) for 10 mins setting the ultrasonic amplitude to 65%. Protein concentration was then estimated using the Qubit® Protein Assay Kit (Life Technologies, Zurich, Switzerland). For each sample, 30 µg of proteins were taken and used for on-filter digestion using an adaptation of the filter-aided sample preparation (FASP) protocol (Wisniewski et al., 2009). Briefly, proteins were diluted in 200 µL of UT buffer (Urea 8 M in 100 mM Tris/HCL pH 8.2), loaded on Ultracel 30000 MWCO centrifugal unit (Amicon Ultra, Merck, Darmstadt, Germany) and centrifuged at 14000*g*. SDS buffer was exchanged by one centrifugation round of 200 µL UT buffer. Alkylation of reduced proteins was carried by 5 min incubation with 100 µL iodoacetamide 0.05 M in UT buffer, followed by three 100 µL washing steps with UT and three 100 µL washing steps with NaCl 0.5 M. Finally, proteins were on-filter digested using 120 µL of 0.05 Triethylammonium bicarbonate buffer (pH 8) containing trypsin (Promega, Madison, WI, USA) in ratio 1:50 (w/w). Digestion was performed overnight in a wet chamber at room temperature. After elution, the solution containing peptides was acidified to a final 0.1% TFA, 3% acetonitirile concentration. Peptides were desalted using Finisterre SPE C18 columns (Teknokroma, Barcelona, Spain), dried and re-solubilized in 15 µL of 3% acetonitrile, 0.1% formic acid for MS analysis.

2.6.2. Liquid chromatography-mass spectrometry analysis

Mass spectrometry analysis was performed on a QExactive mass spectrometer coupled to a nano EasyLC 1000 (Thermo Fisher Scientific). Solvent composition at the two channels was 0.1% formic acid for channel A and 0.1% formic acid, 99.9% acetonitrile for channel B. For each sample 4 µL of peptides were loaded on a self-made column (75 µm × 150 mm) packed with reverse-phase C18 material (ReproSil-Pur 120 C18-AQ, 1.9 µm, Dr. Maisch GmbH) and eluted at a flow rate of 300 nL/min by a gradient from 2 to 35% B in 80 min, 47% B in 4 min and 98% B in 4 min. Samples were acquired in a randomized order. The mass spectrometer was operated in data-dependent mode (DDA), acquiring a full-scan MS spectra (300–1700 *m/z*) at a resolution of 70000 at 200 *m/z* after accumulation to a target value of 3000000, followed by HCD (higher-energy collision dissociation) fragmentation on the twelve most intense signals per cycle. HCD spectra were acquired at a resolution of 35000 using normalized collision energy of 25 and a maximum injection time of 120 ms. The automatic gain control (AGC) was set to 50000 ions. Charge state screening was enabled and singly and unassigned charge states were rejected. Only precursors with intensity above 8300 were selected for MS/MS (2% underfill ratio). Precursor masses previously selected for MS/MS measurement were excluded from further selection for 30 s, and the exclusion window was set at 10 ppm. The samples were acquired using internal lock mass calibration on *m/z* 371.1010 and 445.1200. The mass spectrometry proteomics data have been deposited to the ProteomeXchange Consortium via the PRIDE (Vizcaino et al., 2016) partner repository with the dataset identifier PXD007538.

2.7. MeDIP-Seq analysis

MeDIP-seq analysis was performed according to the protocol of Wolters et al. (Wolters et al., 2017). The dataset was divided into eight different groups of duplicates: (1, 3, 5) Co_MeDIP_1d, Co_MeDIP_2d, and Co_MeDIP_3d, includes the sequencing data of PHHs daily exposed during 1, 2, and 3 day(s), respectively, to the control vehicle; (2, 4, 6) VPA_MeDIP_1d, VPA_MeDIP_2d, and VPA_MeDIP_3d, includes the sequencing data of PHHs exposed for 1, 2, and 3 day(s) daily, respectively, to VPA; (7) Co_MeDIP_6dWO contains the sample exposed for 3 days daily with the vehicle control followed by a WO-period of 3 days; and (8) VPA_MeDIP_6dWO includes the sequencing data of PHHs exposed for 3 days daily to VPA followed by a WO-period of 3 days.

2.8. MRNA-seq analysis

mRNA-seq analysis were performed as early described by Caiment et al. (2015) with minor adjustments (Caiment et al., 2015). In short, mRNA-seq reads were first trimmed to the first 88 bp with Trimmomatic v0.33 and then aligned to the Ensembl human genome (hg38) using Bowtie v1.1.1 (Langmead et al., 2009) using the default parameters. The mapping was then sorted by RSEM v1.2.28 (Li and Dewey, 2011) which provided a read count for all the main gene and known isoforms annotated in the Ensembl genome using expectation-maximization algorithm. Genes and/or isoforms were considered significantly changed if the Benjamini-Hochberg adjusted *p*-value (treated versus time-matched controls) was below 0.05 by using DESeq2.

2.9. Protein identification and label free protein quantification (Protein analysis)

The acquired raw MS data were processed by MaxQuant (version 1.4.1.2), followed by protein identification using the integrated Andromeda search engine. Each file is kept separate in the experimental design to obtain individual quantitative values. Spectra were searched against a forward Swiss Prot-human database, concatenated to a reversed decoyed fasta database and common protein contaminants (NCBI taxonomy ID9606, release date 2015-09-15). Carbamidomethylation of cysteine was set as fixed modification, while methionine oxidation and N-terminal protein acetylation were set as variable. Enzyme specificity was set to trypsin/P allowing a minimal peptide length of 7 amino acids and a maximum of two missed-cleavages. Precursor and fragment tolerance was set to 10 ppm and 20 ppm, respectively for the initial search. The maximum FDR was set to 0.01 for peptides and 0.05 for proteins. Label free quantification was enabled and a 2 min window for match between runs was applied. The requantify option was selected. For protein abundance the intensity (Intensity) as expressed in the protein groups file was used, corresponding to the sum of the precursor intensities of all identified peptides for the respective protein group. Only quantifiable proteins (defined as protein groups showing two or more razor peptides) were considered for subsequent analyses. Protein expression data were transformed (hyperbolic arcsine transformation) and missing values (zeros) were imputed using the missForest R-package (missForest: Nonparametric Missing Value Imputation using Random Forest, R package version 1.4) (Stekhoven, 2013). The protein intensities were normalized by scaling the median protein intensity in each sample to the same values.

For the two-group analysis the statistical testing was performed using *t*-test (treated versus time-matched controls) on transformed protein intensities (hyperbolic arcsine transformation). Proteins were called significantly differentially expressed if linear fold-change exceeded 1.5-fold and the *p*-value from the *t*-test was below 0.05.

2.10. Selection of co-expressed genes and proteins

For the differentially expressed genes (DEGs) at day 1 we selected the genes if the corresponding protein appeared to have changed in the same direction at any of the time-points.

2.11. Selection of persistent genes, proteins, and methylated regions

Genes were selected as persistently upregulated if they were

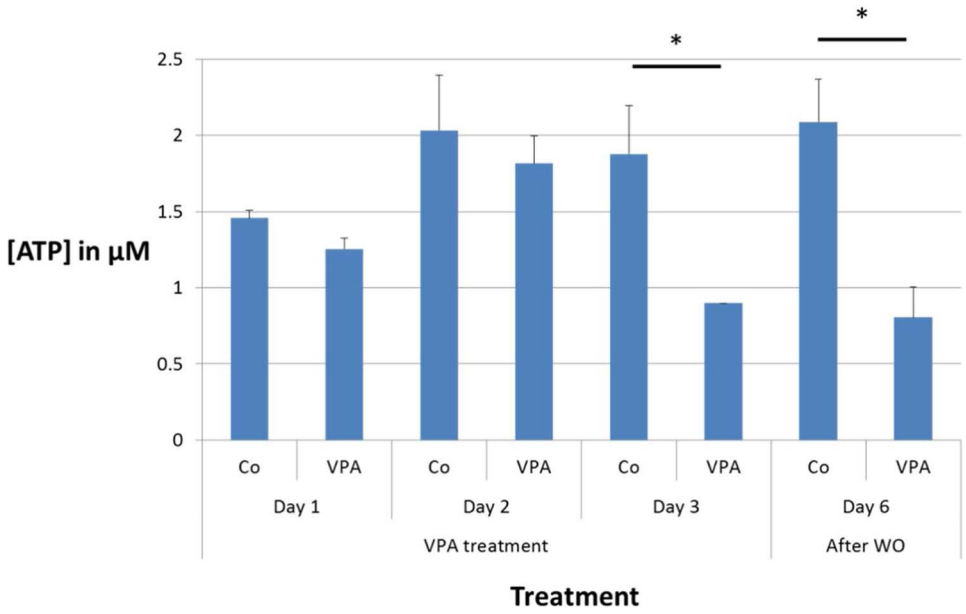

Fig. 2. ATP levels in µM after 1, 2, and 3 days of daily exposure of PHHs to 15 mM VPA, as well as after a 3 day WO-period.

significantly upregulated after 6 days (after the WO-period) and 1) after 3 days of VPA-treatment, or 2) after 2 and 3 days of VPA-treatment, or 3) after 1, 2, and 3 days of VPA-treatment. The same was done for the downregulated genes.

The persistent proteins were defined in the same way as the persistent genes. Methylated regions were selected in the same way but those were divided into hypo- and hypermethylation.

2.12. Pathway analysis

Significantly methylated regions per day, unique differentially expressed genes per day and significantly modified proteins per day were uploaded onto VENNY (Oliveros, 2007). ConsensusPathDB (Kamburov et al., 2011) was used to identify and visualize the involvement of the unique and overlapping genes in biological processes that may be affected on the level of pathways, by selecting significantly perturbed pathways with a p-value < 0.01 from a gene enrichment analysis.

2.13. Network visualization of genes after VPA-treatment

Related genes from the selected significant proteins after VPA-treatment and the WO-period were exported and unique genes were uploaded onto the induced network module of ConsensusPathDB (Kamburov et al., 2011). After that, the protein interactions, with the high-confidence filter, and the gene regulatory interactions (do not allow for intermediate nodes) were exported. This data was then uploaded onto Cytoscape. The circular layout was selected and the network was analyzed as undirected. Fold Change (FC) data were added and nodes were colored (green = gene expression upregulation (positive FC) and red = gene expression downregulation (negative FC)). A selection of hub-genes which show a high number of interactions with other genes (neighbors) was visualized in subnetworks in more detail.

The genes with 5 or more neighbors (connections with other genes in the network) were selected as hub genes. This was done for all the 4 time-points. Then, the hub genes per day were uploaded onto VENNY (Oliveros, 2007) to observe the overlap between the networks.

In addition, interaction network between the genes of different lists was generated by using ToppCluster (Kaimal et al., 2010).

2.14. TSNI ODE protein–protein and gene–gene interaction networks

Protein expressions and VOOM-transformed gene expressions (since ODE TSNI analysis will not work with read counts (RNA-seq data) it needs to be VOOM-transformed to log-counts per million with associated precision weight (Law et al., 2014)) of the genes and proteins of the predefined 'regulation of lipid metabolism' pathway, induced during VPA-treatment and after the washout period, were used for the TSNI ODE analysis. Thereafter, interaction networks were formed by using a p-value < 0.1 as threshold.

2.15. Intracellular ATP measurement in PHHs

The CellTiter-Glo Luminescent Cell Viability Assay (Promega) was performed according to the manufacturer's instructions. In short, PHHs were cultured in a double collagen layer in 96-well plates at a concentration of 0.7*10^6 cells/mL. Background luminescence was taken into account by using wells without cells. Luminescence was measured by using the GloMAx 96 Microplate Luminometer (Promega) and analysed by using the GloMax 96 Software (Promega).

3. Results

3.1. Cytotoxicity and ATP-production

Firstly we showed 77% cell viability (IC_{20}) after 3 days of daily treatment with 15 mM VPA, while this drops to 50% with 20 mM VPA (Fig. 1C). Afterwards, three days of daily VPA-treatment with 15 mM resulted in a decreased ATP-production compared to the control samples thus indicating VPA-induced mitochondrial impairment (Fig. 2). Three days after terminating VPA-treatment this decreased ATP-production appeared still present (Fig. 2).

3.2. DMRs, DEGs and DEPs

3.2.1. Nuclear genomic effects during VPA-treatment and after the washout period

VPA-treatment of PHHs resulted in significant DNA-methylation changes, mRNA gene expression changes, and protein expression changes as determined after 1, 2, and 3 days of exposure. Part of these changes remained persistent after a washout of 3 days. Fig. 3 and

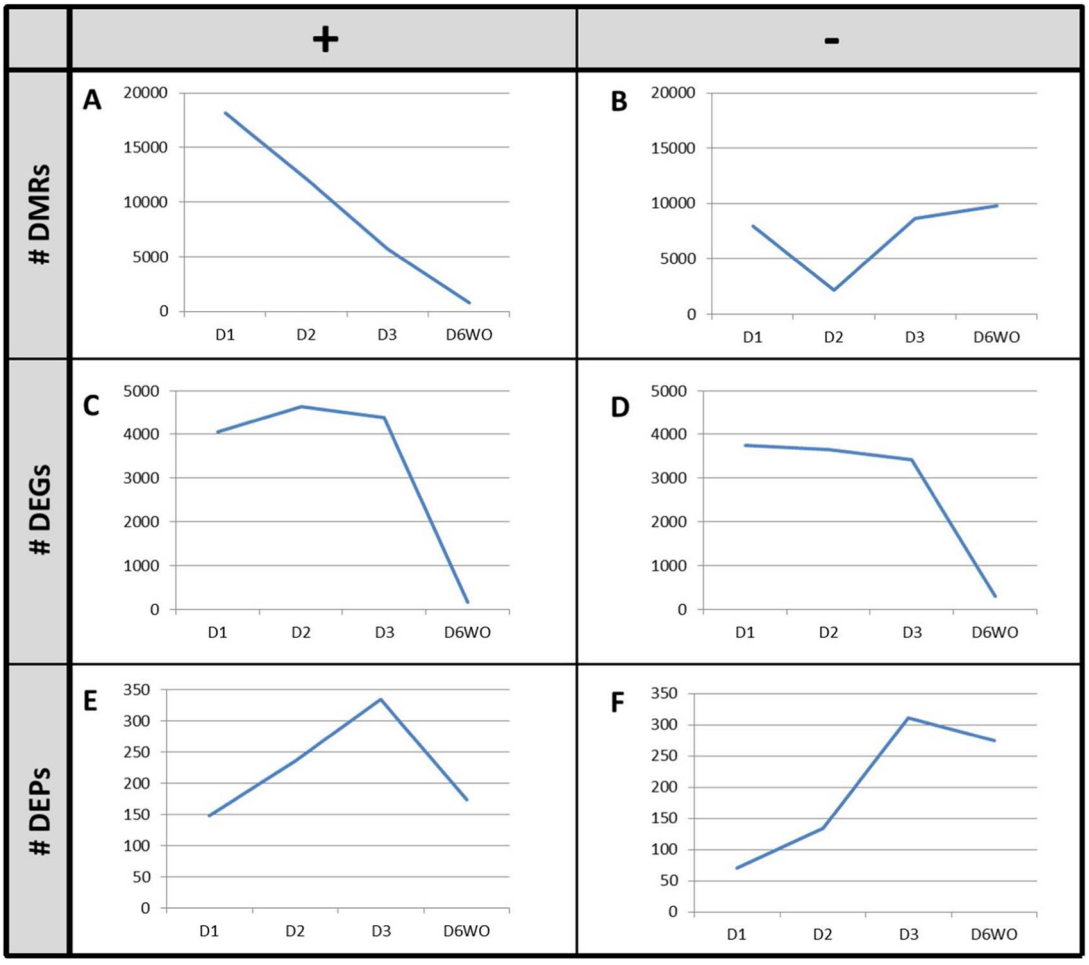

Fig. 3. Numbers of DMRs, DEGs, and DEPs after exposure of PHHs to VPA after 1, 2, and 3 days, as well as after a 3 day WO-period.
A. Number of hypermethylated DMRs after 1 (D1), 2 (D2), and 3 (D3) days, as well as after a 3 day WO-period (D6WO).
B. Number of hypomethylated DMRs after 1 (D1), 2 (D2), and 3 (D3) days, as well as after a 3 day WO-period (D6WO).
C. Number of upregulated DEGs after 1 (D1), 2 (D2), and 3 (D3) days, as well as after a 3 day WO-period (D6WO).
D. Number of downregulated DEGs after 1 (D1), 2 (D2), and 3 (D3) days, as well as after a 3 day WO-period (D6WO).
E. Number of upregulated DEPs after 1 (D1), 2 (D2), and 3 (D3) days, as well as after a 3 day WO-period (D6WO).
F. Number of downregulated DEPs after 1 (D1), 2 (D2), and 3 (D3) days, as well as after a 3 day WO-period (D6WO).
+: DNA hypermethylation, gene expression upregulation, protein expression upregulation;
−: DNA hypomethylation, gene expression downregulation, protein expression downregulation.

Table 1 provide an overview of the numbers of differentially methylated regions (DMRs), differentially expressed genes (DEGs), and differentially expressed proteins (DEPs) at all time points. Numbers of DMRs, DEGs, and DEPs persistently changed into the same direction as apparent after the washout period, are presented in Table 1 (DMRs, DEGs and DEPs) as well as in Figs. 4–6 (19 persistently hypomethylated DMRs (Fig. 4), 206 persistent DEGs (Fig. 5), and 80 persistent DEPs (Fig. 6). In view of the fact that a total of 10579 DMRs was induced after the WO-period, the number of 19 persistently methylated DMRs seems negligibly low and this indicates that VPA-induced nuclear methylome changes are highly reversible.

In particular, in correspondence with the known action of VPA as a HDAC inhibitor, we found multiple effects on the expression levels of genes from the HDAC family which then again normalized after the WO

Table 1
Total number of DMRs, DEGs and DEPs after the daily exposure of PHHs to VPA after 1 [(A)], 2 [(B)] and 3 days [(C)], and after 3 days daily exposure of PHHs with VPA followed by a 3 day WO-period [(D)]. The persistent number of DMRs, DEGs and DEPs after 3 days daily exposure of PHHs with VPA followed by a 3 day WO-period [(E)].

	1-day daily VPA exposure			2-days daily VPA exposure			3-days daily VPA exposure			3-days washout period after 3-days daily VPA exposure					
	Total [(A)]			Total [(B)]			Total [(C)]			Total [(D)]			Persistent [(E)]		
	DMRs	DEGs	DEPs	DMRs	DEGs	DEPs	DMRs	DEGs	DEPs	DMRs	DEGs	DEPS	DMRs	DEGs	DEPs
+	18183	4060	148	12152	4632	236	5716	4391	334	766	154	173	0	68	40
−	7930	3746	70	2182	3651	134	8633	3427	311	9813	291	275	19	138	40
Total	26113	7806	218	14334	8283	370	14349	7818	645	10579	445	448	19	206	80

*direction of effect.
+ = DNA hypermethylation; gene expression upregulation; protein expression upregulated.
− = DNA hypomethylation; gene expression downregulation; protein expression downregulated.

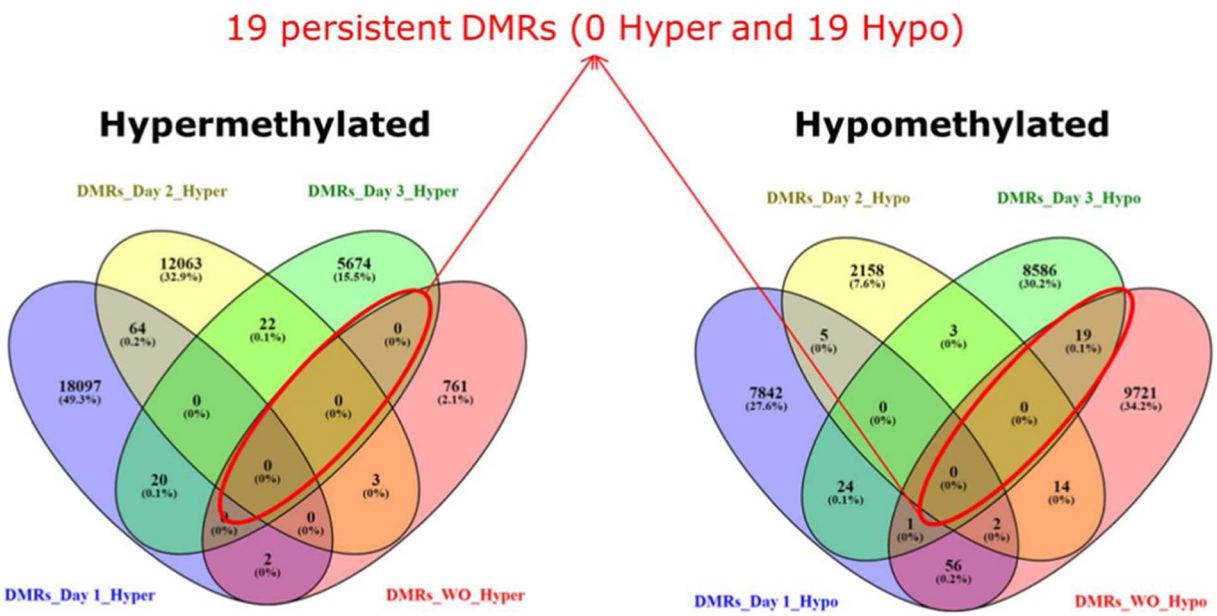

Fig. 4. Venn diagrams of persistently hyper- and hypomethylated DMRs after 1, 2, and 3 days of exposure of PHHs to VPA, as well as after a 3 day WO-period.

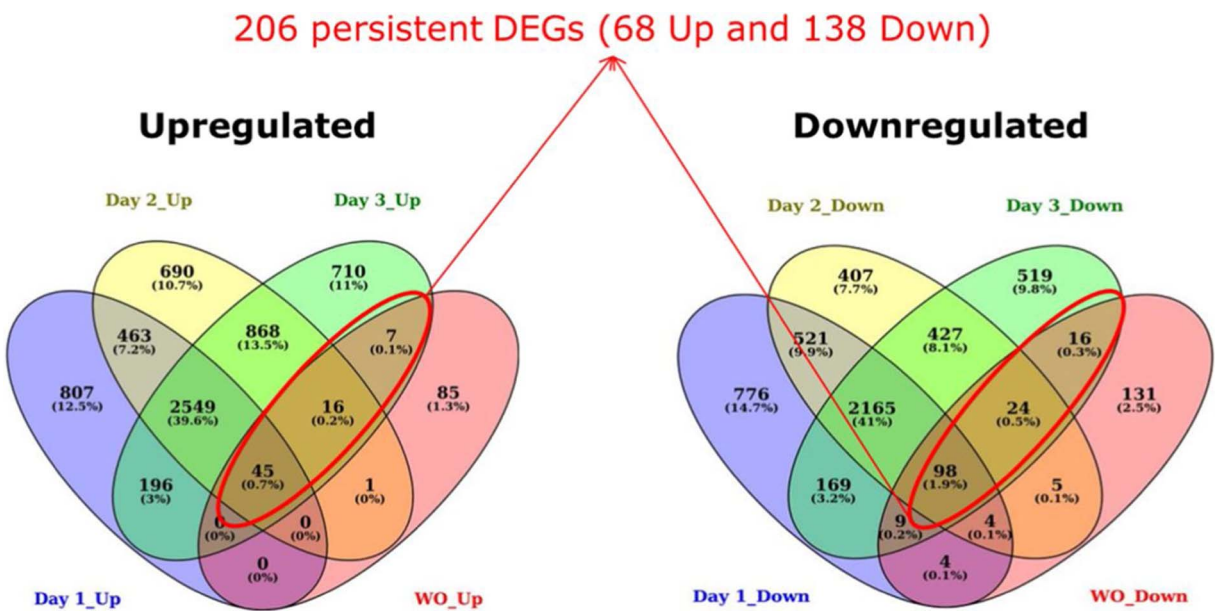

Fig. 5. Venn diagrams of persistently upregulated and downregulated DEGs after 1, 2, and 3 days of exposure of PHHs to VPA, and after a 3 day WO-period.

period.

3.2.2. Mitochondrial genomic effects during VPA-treatment and after the washout

We detected significantly changed methylation patterns for 24 mitochondrial genes which appeared reversible after the WO-period (Supplementary Table S3A). Nine DMRs demonstrated relatively transient increases in methylation levels culminating after 2 days of VPA-treatment (Supplementary Table S3A). For these genes, we noted concordance between DNA hypermethylation and downregulated gene expression.

We found 13 significantly expressed mitochondrial protein-coding genes (as confirmed by MitoCarta2.0 (Calvo et al., 2016)) comprising 2 ATP synthases (*MT-ATP6* and *MT-ATP8*; complex V enzyme of the ETC), 3 cytochrome C oxidases (*MT-CO1*, *MT-CO2*, and *MT-CO3*; complex IV of the ETC), 1 cytochrome b (*MT-CYB*; complex III of the ETC), and 7 NADH dehydrogenase subunits (*MT-ND1*, *MT-ND2*, *MT-ND3*, *MT-ND4*, *MT-ND4L*, *MT-ND5*, and *MT-ND6*; complex I of the ETC). Gene functions refer to maintaining mitochondrial metabolism. All 13 genes showed a decreased expression after 1, 2, and 3 days of daily VPA-treatment (Supplementary Table S3A), which is in line with the observed decreased ATP-production during VPA-treatment (Fig. 2). After the WO-period, these 13 genes were neither up- nor downregulated. Also 2 ribosomal RNAs (*MT-RNR1* (small subunit) and *MT-RNR2* (large subunit)) were significantly expressed during VPA-treatment while the *MT-RNR2* gene was persistently downregulated after washout.

In addition, the proteins of *MT-ATP6*, *MT-CO2*, *MT-ND1*, and *MT-ND4* were detected, showing a trend towards downregulation upon VPA-treatment and after the WO albeit not significantly (Supplementary Table S3A).

3.2.3. ATP-synthases

From the 25 known ATP-synthases (23 nuclear ATP-synthases and 2 mitochondrial ATP-synthases (*MT-ATP6* and *MT-ATP8*)), 17 proteins

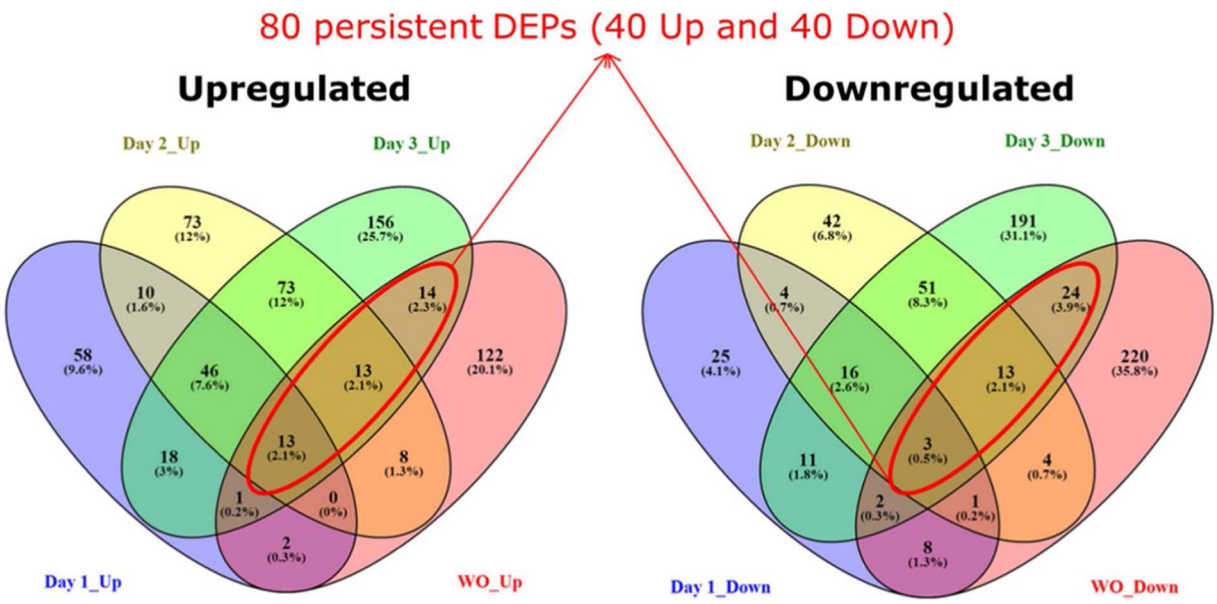

Fig. 6. Venn diagrams of persistently upregulated and downregulated DEPs after 1, 2, and 3 days of exposure of PHHs to VPA, and after 3 days daily exposure of PHHs with VPA followed by a 3 day WO-period.

were detected during VPA exposure; only ATP5S appeared significantly downregulated after 1 day of VPA-treatment (Supplementary Table 1B). In addition, ATP5I and ATP5L were downregulated after the WO-period (Supplementary Table S3B). Interestingly, the expressions of 7 genes coding for ATP-synthases (5 nuclear ATP-synthases: *ATP5B*, *ATP5G2*, *ATP5J*, *ATP5J2*, and *ATP6*; and 2 mitochondrial ATP-synthases: *MT-ATP*-6, and *MT-ATP8*) were significantly downregulated during VPA-treatment and returned to control levels after the WO (Supplementary Table S3B). In addition, DNA methylation patterns were in concordance with gene expression changes for the genes *ATP5 B* (at day 2), *ATP5G2* (at day 1), and *ATP6AP2* (at day 3) during VPA-treatment but appeared reversible after the WO (Supplementary Table S3B). These results match with the observed decrease in ATP-production (Fig. 2).

3.3. Increasing complexity in gene–gene interaction networks during VPA-treatment

Fig. 7A–C demonstrates the increasing complexity of gene–gene interactions for differentially expressed protein-coding genes with the duration of VPA-treatment. This faded out to some degree after washout (Fig. 7D). Pathway analysis of those DEGs connected to 5 or more neighbors showed that predominantly TCA-cycle-related pathways were affected after 3 days of VPA-treatment while mainly pathways involved in ETC, TCA-cycle, fatty acid, and β-oxidation appeared induced after washout (Supplementary Table S4A). The intersection between these networks is shown in Fig. 7E and Supplementary Table S4B. In detail, we found 1 DEG (ENSG00000115414, fibronectin 1 (*FN1*)) initially connected to 10 neighbors which developed 71 connections after 3 days of VPA-treatment while maintaining 50 interactions with neighbor genes after the washout. Similar patterns of developing increasing numbers of gene–gene interactions during VPA treatment, be it lesser than for *FN1*, were observed for IQ motif containing GTPase activating protein 1 (*IQGAP1*), GNAS complex locus (*GNAS*), filamin A (*FLNA*), sequestosome 1 (*SQSTM1*), and caveolin 1 (*CAV1*). Five of the 6 genes (except of *GNAS*), which showed an increased complexity in their gene–gene interaction networks during VPA-treatment, are known to play a role in mitochondria formation and functioning (see Discussion). The neighbor-genes of these 6 genes after 1 and 3 days of VPA-treatment are listed in Supplementary Table S4B-H.

In summary, 2 of the 5 nuclear genes which showed an increased complexity in their gene–gene interactions over time during VPA-treatment and which were all involved in mitochondrial function (namely, FN1 and IQGAP1), were identified as important hub genes which remained persistently changed during washout. This seemed not related to any modification in the temporal methylation patterns of these genes. In addition, we have found the neighbor-genes nudix hydrolase 21 (*NUDT21* (neighbor of *FN1*)), insulin like growth factor 2 receptor (*IGF2R* (neighbor of *FN1*)), SMAD family member 3 (*SMAD3* (neighbor of *FLNA* and *SQSTM1*)), inhibitor of nuclear factor kappa B kinase subunit gamma (*IKBKG* (neighbor of *FLNA* and *SQSTM1*)), and PYD and CARD domain containing (*PYCARD* (neighbor of *SQSTM1*)) in the list of 137 unique DEGs which demonstrated an increasing concordance with protein expression over time (see the next paragraph).

3.4. Concordance in time between transcriptome and proteome expression during VPA-treatment and after the washout

Co-expression between DEGs and their corresponding DEPs increased over time (Supplementary Fig. S1A). The percentage of DEGs upregulated in concordance with their DEPs increased from 2.0% to 5.2% after the WO-period (Supplementary Fig. S1A). Concordance between downregulated DEGs and their corresponding DEPs appeared much more substantial, namely from 8.6% at day 1 to an astonishing 26% after the WO-period (Supplementary Fig. S1A). The same trend was shown for DEGs at day 2 and day 3.

Pathway analysis of the 137 unique DEGs, which demonstrated concordance with protein expression over time, returned 106 significantly enriched pathways (Supplementary Table S5). 109 DEGs appeared present in at least one pathway. Interestingly, 32 out of these 106 pathways refer to 1) VPA metabolism (such as Valproic acid pathway), 2) Pyruvate deficiency (such as Pyruvate Metabolism), 3) fatty acid metabolism-associated pathways (such as Fatty Acid Omega Oxidation; Regulation of lipid metabolism by Peroxisome proliferator-activated receptor alpha (PPARalpha); Mitochondrial LC-Fatty Acid Beta-Oxidation; Fatty Acid Beta Oxidation; Metabolism of lipids and lipoproteins; Fatty acid degradation; Nuclear Receptors in Lipid Metabolism and Toxicity), and 4) ATP-associated pathway (such as Glycolysis Gluconeogenesis). Methylation changes of some genes (notably *MAOB*, *PYCARD*, *GSDMD*, *PPIF*, *SMAP1*, *TTPA*, *ASGR1*, *PKLR*, *AK4*, *FBP1*, *ARF6*, *SUGCT*, *ACSM2A*, and *TBC1D9B*) were in concordance with their expression and protein changes (Supplementary

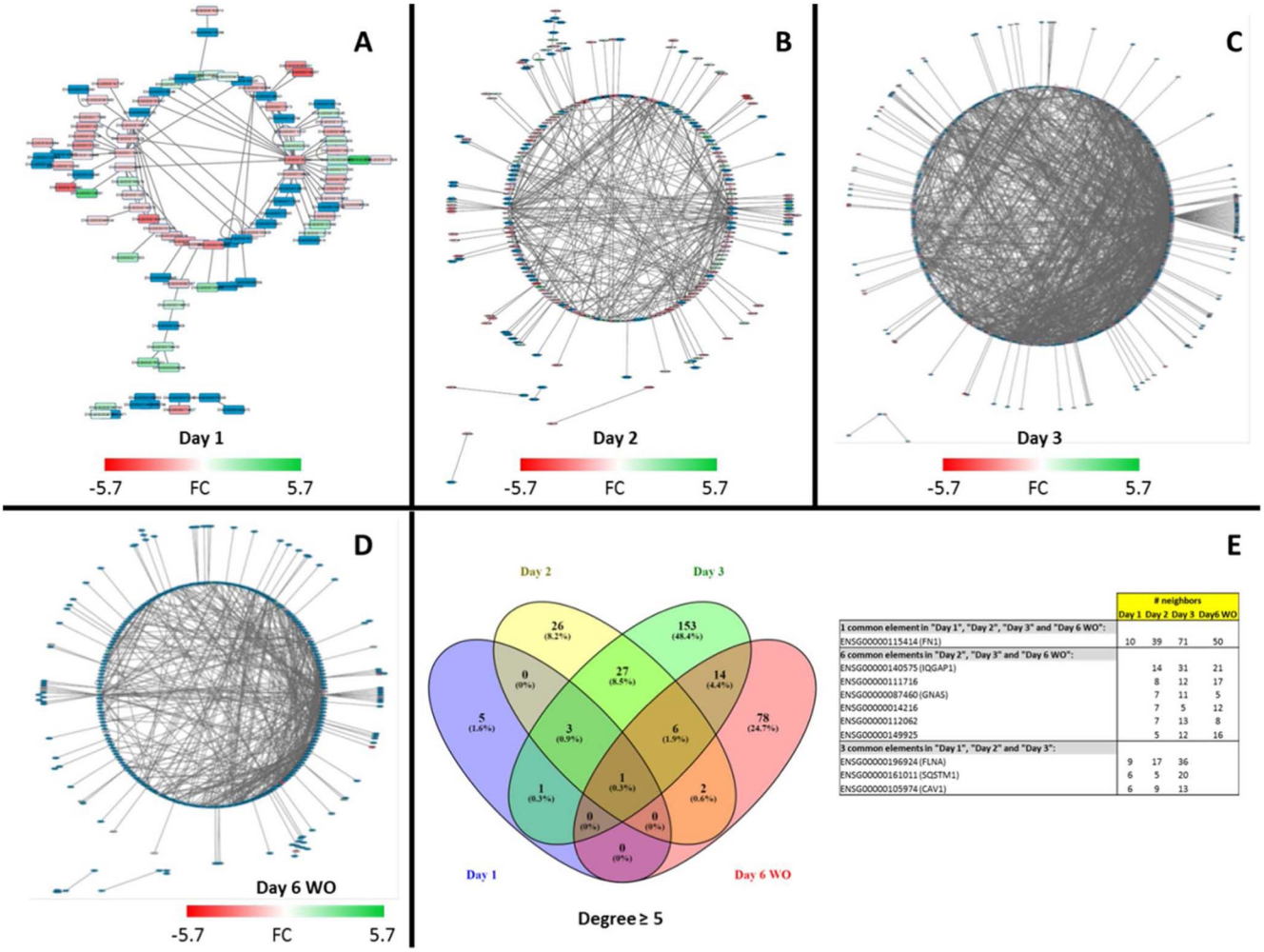

	# neighbors			
	Day 1	Day 2	Day 3	Day6 WO
1 common element in "Day 1", "Day 2", "Day 3" and "Day 6 WO":				
ENSG00000115414 (FN1)	10	39	71	50
6 common elements in "Day 2", "Day 3" and "Day 6 WO":				
ENSG00000140575 (IQGAP1)		14	31	21
ENSG00000111716		8	12	17
ENSG00000087460 (GNAS)		7	11	5
ENSG00000014216		7	5	12
ENSG00000112062		7	13	8
ENSG00000149925		5	12	16
3 common elements in "Day 1", "Day 2" and "Day 3":				
ENSG00000196924 (FLNA)	9	17	36	
ENSG00000161011 (SQSTM1)	6	5	20	
ENSG00000105974 (CAV1)	6	9	13	

Fig. 7. Cytoscape generated dynamic molecular interaction networks after exposure of PHHs to VPA after 1, 2, and 3 days, as well as after a 3 day WO-period.
A. Dynamic network of 218 genes concordantly expressed in relation of their significantly differentially expressed proteins (DEPs) in PHHs after 1 day of VPA-treatment.
B. Dynamic network of 370 genes concordantly expressed in relation of their significantly differentially expressed proteins (DEPs) in PHHs after 2 days of VPA-treatment.
C. Dynamic network of 645 genes concordantly expressed in relation of their significantly differentially expressed proteins (DEPs) in PHHs after 3 days of VPA-treatment.
D. Dynamic network of 448 genes concordantly expressed in relation of their significantly differentially expressed proteins (DEPs) in PHHs after WO-period.
E. Venn diagram showing the overlap of genes with 5 or more interactions in the networks of Day 1 (**A**), Day 2 (**B**), Day 3 (**C**), and Day 6 WO (**D**), with some DEGs emphasized in Table next to the venn diagram.
Legend (A–D): green = gene expression upregulation; red = gene expression downregulation.

Table S6A).

Interestingly, 38 genes expressed in concordance with their proteins and identified in the overlap of these 32 pathways, overall showed a downregulation in mRNA expression during VPA-treatment followed by a downregulation of the corresponding protein during the WO-period (Supplementary Table S6B). These 38 genes predominantly refer to acyl-CoA synthetase medium-chain family members (ACSM; *ACSM5*, *ACSM2A*, and *ACSM2B*) which are catalyzers of the oxidation of VPA to VPA-CoA in the mitochondria, cytochrome P450 enzymes (CYPs; *CYP4A11*, *CYP2E1*, *CYP2C8*, *CYP4F3*, *CYP2D6*, *CYP8B1*, and *CYP2C9*) which are involved in VPA-metabolism, alcohol dehydrogenases (ADH; *ADH1C* and *ADH4*) which play a role in the Glycolysis Gluconeogenesis (ATP-associated pathway), carnitine palmitoyltransferases (CPT; *CPT1A* and *CPT2*), 3-hydroxy-3-methylglutaryl-CoA synthase 2 (*HMGCS2*), and acyl-CoA oxidases (ACOX; *ACOX1* and *ACOX2*). Consequently, the observed co-expression of these genes with their proteins points towards a downregulation of VPA-metabolism, as well as a downregulation of ATP synthesis, also after the washout period. Finally, the methylation patterns of these 38 genes demonstrated concordance with the expression of *ACSM2A*, monoamine oxidase B (*MAOB*), ATP binding cassette subfamily C member 2 (*ABCC2*), solute carrier family 25 member 20 (*SLC25A20*), and fructose-bisphosphatase 1 (*FBP1*). Furthermore, 11 of the 38 genes selected from the 32 pathways described before, have previously been identified as genes that encode for mitochondrial proteins (such as *CPT1A*, *CPT2*, and *ACSM5*) by using MitoCarta2.0 (Calvo et al., 2016). In addition, from the in total 137 concordant DEGs with their DEPs we have found 38 genes which encode for mitochondrial proteins as identified by MitoCarta2.0 (Calvo et al., 2016) (Supplementary Table S6C).

3.5. TSNI ODE protein–protein and gene–gene interaction networks

TSNI disclosed a small protein–protein interaction network induced during VPA treatment, within the 'regulation of lipid metabolism' pathway, which appeared composed from 7 proteins targeting the downregulated perilipin2 (PLIN2) (Supplementary Fig. S2). TSNI did not reveal any significant gene–gene interaction networks during VPA-treatment within the 'regulation of lipid metabolism' pathway. Furthermore, the addition of the washout period to the protein or gene TSNI analysis did not reveal any further significant protein–protein or gene–gene interaction network.

3.6. Pathway analysis of persistent DEGs and DEPs

As mentioned before we deem the presence of 19 persistently methylated DMRs negligible. Consequently, for further analyses of persistence of VPA-induced molecular events we focused on DEGs and DEPs which remained expressed into the same direction after WO. Pathway analysis of the 206 persistent DEGs (of which 68 were upregulated and 138 downregulated) returned 104 significantly enriched pathways (Supplementary Table S7A). Among these, some refer to VPA metabolism (such as Valproic Acid Metabolism Pathway), Pyruvate deficiency (such as Pyruvate Dehydrogenase Complex Deficiency; Pyruvate kinase deficiency; Pyruvate Metabolism; Pyruvate Decarboxylase E1 Component Deficiency (PDHE1 Deficiency)), and fatty acid metabolism-associated pathways (such as Fatty Acid Omega Oxidation; Fatty acid biosynthesis − Homo sapiens (human); Regulation of lipid metabolism by Peroxisome proliferator-activated receptor alpha (PPARalpha); Lipid digestion, mobilization, and transport; Metabolism of lipids and lipoproteins; Nuclear Receptors in Lipid Metabolism and Toxicity).

The 80 persistent DEPs (of which 40 were upregulated and 40 downregulated) were classified into 100 significantly enriched pathways (Supplementary Table S7B). These 100 pathways predominantly refer to the endogenous metabolism but to some extent also to VPA metabolism (such as Valproic Acid Pathway Pharmacodynamics and Valproic Acid Pathway Pharmacokinetics (Supplementary Table S8A–C)), and fatty acid metabolism-associated pathways (such as Saturated fatty acids beta-oxidation (Supplementary Table S8D and E)).

4. Discussion

In the present study, we performed whole genome analysis of DNA-methylation, gene expression, and protein expression in PHHs induced by VPA, thereby focusing on the concordance between results from these three platforms and on the persistence of induced changes, in particular with respect to VPA-induced mitochondrial toxicity. Reduced ATP-production also after WO (Fig. 2), confirms VPA-induced persistent mitochondrial dysfunction in PHHs. In addition, thousands of DMRs were found after 1, 2, and 3 days of VPA-treatment. After the WO-period not more than 19 DMRs appeared persistently hypomethylated thus indicating strong reversibility of VPA-induced epigenomic alterations (Figs. 3 and 4). While considerable reversibility of VPA-induced gene and protein expression was also demonstrated after washout, pathway analysis of significantly and persistently expressed genes and proteins returned processes which refer to VPA metabolism, pyruvate deficiency, fatty acid metabolism-associated pathways, and ATP-associated pathways, in correspondence to the observed reductions in ATP production.

For cross-omics analysis, we initially considered an unsupervised data integration (such as ICluster+ (Mo et al., 2013) and Bayesian tensor factorization (Khan et al., 2016)), which however did not work out in our datasets, because of a) skewness of the data distribution in view of the limited sample numbers, and b) known resolution differences between the 'omics platforms. Therefore, we continued with time-resolved supervised data integration, by using a network-based approach based on ODE (Hendrickx et al., 2017), thereby exploiting the predefined "regulation of lipid metabolism" pathway as *a priori* knowledge. In particular, for capturing temporally induced network motifs, we used Time Series Network Identification (TSNI) (Bansal et al., 2006) based on ODE, describing the time evolution of the expression of each gene which is dependent on the expression of other genes. TSNI on samples during VPA treatment disclosed a small protein–protein interaction network, targeting PLIN2, within the 'regulation of lipid metabolism' pathway. PLIN2 is associated with intracellular lipid accumulation but appeared increasingly downregulated across time. By contrast, TSNI did not reveal any significant gene–gene interaction networks during VPA-treatment. We suggest that this is due to the extreme dynamics of the transcriptome response to VPA (Fig. 7).

This discordance may to some extent reflect protein-level buffering of coexpressed genes, spatially closed neighboring genes described earlier, thereby putting limitations to the functional analysis of cross-omics responses (Kustatscher et al., 2017). Consequently, we deemed this ODE-based approach not quite satisfactory in this particular case.

As a next step, we used a data-based approach thereby inferring the topology of inter-linked gene networks from known interactions (Le Novere, 2015).

VPA is known as a HDAC-inhibitor e.g. via proteosomal degradation of *HDAC2* (Kramer et al., 2003). We found downregulation of *HDAC6* (day 1) and *HDAC7* (day 1, day 2, and day3), as well as upregulation of *HDAC1, HDAC3* and *HDAC9*. Inhibition of *HDAC7* by VPA was found in previous studies (Gurvich et al., 2004; Kwiecinska et al., 2014). Where HDAC inhibition has been reported to be associated with specific DNA hypomethylation (Sarkar et al., 2011) as well as with global hypermethylation (Gu et al., 2012), we have previously demonstrated hypo- as well as hypermethylation induced in PHH after 5 days of VPA treatment (Wolters et al., 2017). Here, we observed a gradual demethylation across time (Fig. 3A) but also a transient decrease in hypomethylation culminating on day 2 of VPA administration. Correspondingly, we found downregulation of *DNMT1* after 1 and 2 days of VPA administration but specifically found *DNMT2* expression to be upregulated after 2 and 3 days VPA-treatment, which may explain the transient increases of DNA methylation levels on day 2 in either nDNA and/or mtDNA. In line with this, 9 of the 13 mitochondrial genes coding for proteins (*MT-ATP6*, *MT-CO1*, *MT-CO2*, *MT-CO3*, *MT-CYB*, *MT-ND1*, *MT-ND2*, *MT-ND4*, and *MT-ND5*) showed increased methylation after 2 days of VPA-treatment compared with day 1, which matches with the downregulation of the expression levels of these mitochondrial genes during VPA-treatment. All 9 concordantly methylated and expressed mitochondrial genes refer to a decreased activity in complex I, III, IV, or V of the ETC and this relates to the decreased ATP-production after 3 days of VPA-treatment. Although we do not have a direct explanation for the subsequent decrease in methylation levels of these mitochondrial genes observed on day 3, we observed a slight increase of Tet methylcytosine dioxygenase 1 (*TET1)* expression (log2 FC of −2.1 (day 1) to −1.6 (day 3)) known to actively cause DNA demethylation. All in all, interactions of VPA with the *HDAC* and *DNMT* gene families regulating epigenomic status, seem more complicated than anticipated from literature, and require further in depth investigations.

The persistently decreased ATP-production is a sign of VPA-induced mitochondrial dysfunction most probably reflecting adverse consequences of oxidative stress. This has been suggested to activate a mitochondria-nucleus signaling pathway potentially modulated by 40 identified transcription factors (TFs) which has been hypothesized to counteract the toxicant-induced mitochondrial dysfunction (Jazwinski, 2013; Kotiadis et al., 2014; Ryan and Hoogenraad, 2007). Sixteen out of these 40 TFs were (slightly) increased or decreased at day 2 or day 3 of VPA-treatment (Supplementary Table S9). We thus asked whether these deregulated TF expressions may inform about the observed increasing complexity of gene–gene interactions with the duration of VPA treatment, in particular with regard to the observed mitochondrial toxicity.

Five of the 6 genes (except of *GNAS*), which developed an increasing number of neighbors during VPA-treatment which dropped again after washout (Fig. 7E), play a role in mitochondria formation and functioning (Lehwald et al., 2012; Mukherjee et al., 2014; Schmidt et al., 2008; Seibenhener et al., 2013; Volonte et al., 2016; Wu et al., 2005; Yu et al., 2017). *FN1* knock-down has been shown to induce mitochondrial-dependent apoptosis by decreasing CA^{2+} (Wu et al., 2005). Furthermore, *IQGAP1* is known to play a role in β-catenin expression (Schmidt et al., 2008), which has an important role in mitochondrial homeostasis (Lehwald et al., 2012). In addition, *FLNA* and *CAV1* are required for the transport of ribonucleoprotein to the mitochondria (Mukherjee et al., 2014). *CAV1* has also been shown to reduce the ATP-production via mitochondrial dysfunction (Volonte et al., 2016; Yu

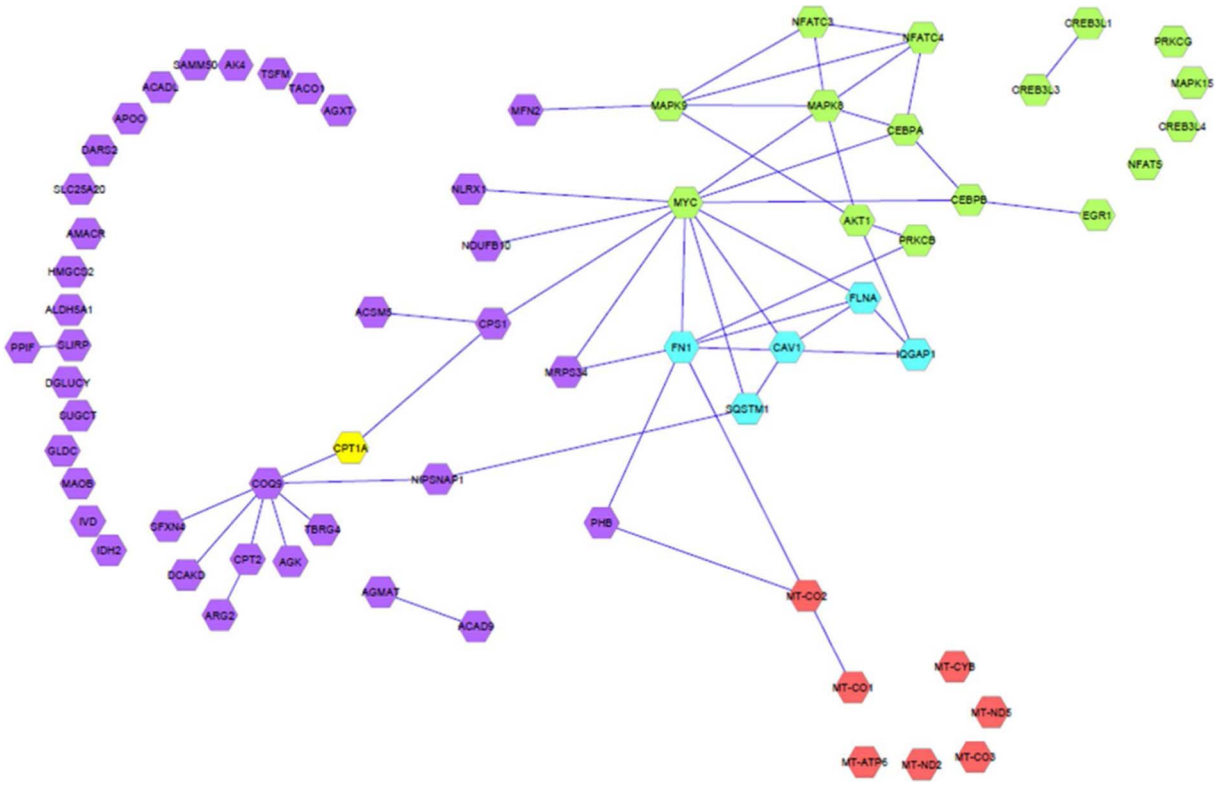

Fig. 8. Interaction network between the genes of 4 different lists by using ToppCluster (Kaimal et al., 2010).
Cluster 1 (red): 7 genes of the mtDNA coding for mitochondrial proteins which have shown concordance between methylation patterns and gene expression; Cluster 2 (blue): 5 genes which have shown increased numbers of neighbors in the networks; Cluster 3 (purple): 38 genes that showed concordance with protein expression and are known to encode for mitochondrial proteins by using MitoCarta2.0 (Calvo et al., 2016); and Cluster 4 (green): 16 transcription factors of the mitochondria-nucleus signaling pathway which have shown modified mRNA expression values after 2 and/or 3 days of VPA-treatment. The concordant gene/protein CPT1A has been marked yellow, since it is the direct target of VPA.

et al., 2017). *SQSTM1* deficiency causes defects in mitochondrial membrane potential which can lead to mitochondrial dysfunction (Seibenhener et al., 2013). Interestingly, the mitochondria-nucleus signaling TF MYC proto-oncogene bHLH transcription factor (*MYC*) interconnected the network building genes *FN1, SQSTM1, CAV1,* and *FLNA* (Fig. 8). Hereby, the downregulated expressions of *FN1, CAV1*, and *FLNA* during VPA-treatment correspond with the downregulation of *MYC* on day 1 and day 2. *MYC* expression had normalized after the WO period, possibly through hypermethylation (Supplementary Table S9).

Most interestingly, in contrast to the earlier hypothesis that it is toxicant-related oxidative stress which activates the mitochondria-nucleus signaling pathway (Jazwinski, 2013; Kotiadis et al., 2014; Ryan and Hoogenraad, 2007) we now propose that mitochondria-nucleus communications result from direct gene–gene interactions induced by VPA (Fig. 8). In more detail, the mitochondrial gene *MT-CO2* interacts with 1 of the 5 network genes, namely *FN1* (directly, as well as indirectly via prohibitin (*PHB*)). This *FN1* seems to play a pivotal role in this interaction network, since it showed also connections with 2 other network genes (namely *CAV1* and *FLNA*) and with 2 TFs involved in the mitochondria-nucleus signaling (namely *PRKCB* and *MYC*). Notably, the importance of *FN1* in the mitochondrial nuclear crosstalk has been noted in a previous study where *FN1* was upregulated in a breast epithelial cell line devoid of mtDNA (ρ^{00} cells) compared to a breast carcinoma cell line (Kulawiec et al., 2008). Furthermore, *MYC* interacts with 3 other TFs relevant for toxicant-induced mitochondria-nucleus signaling, with 4 of the 5 network genes, and most importantly, with 4 genes concordantly regulating mitochondrial proteins.

Lastly, the neighbor-genes *SMAD3* and IKBKG (neighbors of *FLNA* and *SQSTM1*), *IGF2R* (neighbor of *FN1*), and *PYCARD* (neighbor of *SQSTM1*) demonstrated increasing concordance with protein expression over time. *SMAD3* is involved in mitochondria functioning (Yu et al., 2014) and *PYCARD* is known to induce mitochondrial apoptosis (Liu et al., 2012). In addition, the methylation level of *SMAD3* during 1 and 3 days of VPA-treatment corresponds with the mRNA and protein expression. Interestingly, the mitochondria-nucleus signaling TF mitogen-activated protein kinase 14 (*MAPK14*) is present as a neighbor in the complex networks of *IQGAP1*, *FLNA*, and *SQSTM1* after 2 and 3 days of VPA-treatment.

Another important *MYC* target within this mitochondria-nucleus signaling pathway is carbamoyl-phosphate synthase 1 (*CPS1*), which is a phosphorylating enzyme using ATP in the mitochondria. *MYC* and *CPS1* were both downregulated after 1 and 2 days of VPA-treatment. *CPS1* interacts with the downregulated *CPT1A* (which is known to be competitively and non-competitively inhibited by VPA) and induces a network of 6 downregulated concordant genes/proteins (nipsnap homolog 1 (*NIPSNAP1*), transforming growth factor beta regulator 4 (*TBRG4*), acylglycerol kinase (*AGK*), dephospho-CoA kinase domain containing (*DCAKD*), sideroflexin 4 (*SFXN4*), and *CPT2*) via the downregulation of coenzyme Q9 (*COQ9*) at day 1. In addition, the concordant genes *AGK*, *COQ9*, and *CPT2* known to encode for mitochondrial proteins according to MitoCarta2.0 (Calvo et al., 2016) (these proteins were involved in lipid and glycerolipid metabolism (AGK), mitochondrial ubiquinone biosynthesis (COQ9), and oxidizing long-chain fatty acids in the mitochondria (CPT2)) appeared downregulated after the washout.

In addition, 38 genes/proteins were selected from the metabolic pathways that show an increasing concordance between gene and protein expression over time thus indicating an improved regulation of protein expression (a.o. referring to CYPs, CPTs, ACSMs, and uridine 5'diphosphate (UDP)-glucuronosyltransferases (UGTs)). The possible direct inhibitory effect of VPA on CPT1 expression suggests that the normal fatty acid transport into the cell is repressed which may result in a decreased β-oxidation, TCA-cycle, and ETC and finally into a

repressed ATP-production and thus to mitochondrial toxicity. *CPT1* mRNA gene expression was downregulated during VPA-treatment while the protein was only downregulated after washout. This also implies that VPA, being a simple fatty acid itself, may inhibit through *CPT1* downregulation its own transport into the mitochondria and therefore, its own oxidative metabolism. In addition, co-expression between genes and proteins was predominantly found for metabolic enzymes such as ACSMs, UGTs, and CYPs. The controlled downregulation of transporters and enzymes involved in VPA metabolism indicate end-product inhibition, suggesting an adaptation of PHHs to the VPA challenge resulting in a decrease of oxidative VPA metabolite formation.

In summary, our cross-omics analysis of dynamic perturbations caused by the prototypical liver toxicant VPA in human hepatocytes has revealed new insights in the mitochondrial-nuclear crosstalk endorsing VPA-induced mitochondrial toxicity as apparent from reduced ATP production which was maintained even after terminating VPA treatment, as well as reducing oxidative VPA metabolism as an adaptive response to the continuing VPA challenge. We propose that in the early phase of treatment VPA-generated oxidative stress downregulates the electron transport chain and the expression of a range of ATP-synthases which leads to an initial decrease in ATP production as a first manifestation of mitochondrial toxicity. Subsequently, through interference with the HDAC/DNMT gene families, VPA induces a transient hypermethylation which further downregulates mitochondrial genes thus increasingly impairing mitochondrial function and ATP production. One of these mitochondrial genes, *MT-CO2,* thereupon activates the mitochondria-nucleus signaling pathway mediated by *FN1* which over time establishes an interaction with the downregulated nuclear TF *MYC*. Thereafter, *MYC* decreases *CPS1* expression which then downregulates *CPT1A*, proteins of CPS1 and CPT1A being downregulated even after washout. This leads to the downregulation of a small regulatory network consisting of six concordant mitochondrial genes (Fig. 8). This gene–gene interaction network is confirmed by the fact that proteins of CPS1, CPT1A, COQ9, AGK, and CPT2 were downregulated even after terminating VPA treatment which matches with the observed repressed ATP-production after washout (Fig. 2). This impairment of the mitochondrial function has been considered as one of the reasons for steatosis/hepatotoxicity (Begriche et al., 2006; Pessayre et al., 1999; Silva et al., 2008).

5. Conclusions

Through our integrated ‘omics approach, we found relevant concordance between observed VPA-induced transient methylation changes in mtDNA and dynamic downstream responses in relation with decreased ATP-production. This provided us with a deeper insight in the exact cross-omics mechanisms across time upon VPA-treatment and after the washout. We have identified a potential novel mitochondria-nucleus signaling axis, MT-CO2–FN1–MYC − CPT1, which underlies, firstly, VPA-induced mitochondrial dysfunction and, secondly, indicates repressed VPA-metabolism as an adaptation mechanism. Overall, this cross-omics study has for the first time depicted a drug-induced transient effect on the methylation of mtDNA, which through a dedicated mitochondrial-nuclear communication pattern activates an increasingly complex cascade of gene–gene interactions (in mtDNA and nDNA) whereby *MYC* and *FN1* seems to play an extremely important role, finally resulting in a persistent mitochondrial dysfunction. The results from this genome-wide survey of drug-induced responses in human liver cells disclosing novel mechanisms-of action of toxic substances demonstrates the strength of the temporal study design in analyzing effects of impulse perturbations in biological systems. However, an even higher resolution in time is required to unravel the exact sequence of events to greater depth; this is now applied in follow-up studies.

Funding

This research did not receive any specific grant from funding agencies in the public, commercial, or not-for-profit sectors.

Conflict of interest

The authors have no conflicts of interest to declare.

Author contributions

Conceptualization: JEJWolters, SGJvanBreda, FCaiment, JCSKleinjans.
Lab-work DNA and RNA: JEJWolters, SGJvanBreda.
Lab-work Protein: JEJWolters, SGJvanBreda.
Sequencing DNA and RNA: JEJWolters.
LC–MS/MS Protein: CFortes.
Data analysis DNA and RNA: JEJWolters, FCaiment.
Data analysis Protein: JEJWolters, JGrossman.
Supervision: JCSKleinjans, SGJvanBreda.
Writing – original draft: JEJWolters, JCSKleinjans.
Writing – review & editing: JEJWolters, SGJvanBreda, JGrossmann, CFortes, FCaiment, JCSKleinjans.

Acknowledgement

The authors thank the Functional Genomics Center Zurich (FGCZ) for performing the protein measurements and raw-data analysis.

Appendix A. Supplementary data

Supplementary data associated with this article can be found, in the online version, at https://doi.org/10.1016/j.toxlet.2018.02.026.

References

Adachi, T., Nakagawa, H., Chung, I., Hagiya, Y., Hoshijima, K., Noguchi, N., Kuo, M.T., Ishikawa, T., 2007. Nrf2-dependent and −independent induction of ABC transporters ABCC1, ABCC2, and ABCG2 in HepG2 cells under oxidative stress. J. Exp. Ther. Oncol. 6 (4), 335–348.

Aires, C.C., Ijlst, L., Stet, F., Prip-Buus, C., de Almeida, I.T., Duran, M., Wanders, R.J., Silva, M.F., 2010. Inhibition of hepatic carnitine palmitoyl-transferase I (CPT IA) by valproyl-CoA as a possible mechanism of valproate-induced steatosis. Biochem. Pharmacol. 79 (5), 792–799.

Bacalini, M.G., D'Aquila, P., Marasco, E., Nardini, C., Montesanto, A., Franceschi, C., Passarino, G., Garagnani, P., Bellizzi, D., 2017. The methylation of nuclear and mitochondrial DNA in ageing phenotypes and longevity. Mech. Ageing Dev. 165 (Pt B), 156–161. http://dx.doi.org/10.1016/j.mad.2017.01.006. Epub 2017 Jan 20.

Bansal, M., Della Gatta, G., di Bernardo, D., 2006. Inference of gene regulatory networks and compound mode of action from time course gene expression profiles. Bioinformatics 22 (7), 815–822.

Bar-Joseph, Z., Gitter, A., Simon, I., 2012. Studying and modelling dynamic biological processes using time-series gene expression data. Nat. Rev. Genet. 13 (8), 552–564.

Begriche, K., Igoudjil, A., Pessayre, D., Fromenty, B., 2006. Mitochondrial dysfunction in NASH: causes, consequences and possible means to prevent it. Mitochondrion 6 (1), 1–28.

Bugiak, B.J., Weber, L.P., 2010. Phenotypic anchoring of gene expression after developmental exposure to aryl hydrocarbon receptor ligands in zebrafish. Aquat. Toxicol. 99 (3), 423–437.

Caiment, F., Gaj, S., Claessen, S., Kleinjans, J., 2015. High-throughput data integration of RNA-miRNA-circRNA reveals novel insights into mechanisms of benzo[a]pyrene-induced carcinogenicity. Nucleic Acids Res. 43 (5), 2525–2534.

Calvo, S.E., Clauser, K.R., Mootha, V.K., 2016. MitoCarta2.0: an updated inventory of mammalian mitochondrial proteins. Nucleic Acids Res. 44 (D1), D1251–D1257.

Chan, K., Truong, D., Shangari, N., O'Brien, P.J., 2005. Drug-induced mitochondrial toxicity. Expert Opin. Drug Metab. Toxicol. 1 (4), 655–669.

Chang, T.K., Abbott, F.S., 2006. Oxidative stress as a mechanism of valproic acid-associated hepatotoxicity. Drug Metab. Rev. 38 (4), 627–639.

Chen, H., Dzitoyeva, S., Manev, H., 2012. Effect of valproic acid on mitochondrial epigenetics. Eur. J. Pharmacol. 690 (1–3), 51–59.

Dong, E., Chen, Y., Gavin, D.P., Grayson, D.R., Guidotti, A., 2010. Valproate induces DNA demethylation in nuclear extracts from adult mouse brain. Epigenetics 5 (8), 730–735.

Gu, S., Tian, Y., Chlenski, A., Salwen, H.R., Lu, Z., Raj, J.U., Yang, Q., 2012. Valproic acid shows a potent antitumor effect with alteration of DNA methylation in

neuroblastoma. Anticancer Drugs 23 (10), 1054–1066.
Gurvich, N., Tsygankova, O.M., Meinkoth, J.L., Klein, P.S., 2004. Histone deacetylase is a target of valproic acid-mediated cellular differentiation. Cancer Res. 64 (3), 1079–1086.
Hargreaves, I.P., Al Shahrani, M., Wainwright, L., Heales, S.J., 2016. Drug-induced mitochondrial toxicity. Drug Saf. 39 (7), 661–674.
Hendrickx, D.M., Souza, T., Jennen, D.G.J., Kleinjans, J.C.S., 2017. DTNI: a novel toxicogenomics data analysis tool for identifying the molecular mechanisms underlying the adverse effects of toxic compounds. Arch. Toxicol. 91 (6), 2343–2352.
Huang, S., Chaudhary, K., Garmire, L.X., 2017. More is better: recent progress in multi-omics data integration methods. Front. Genet. 8 (84).
Iacobazzi, V., Castegna, A., Infantino, V., Andria, G., 2013. Mitochondrial DNA methylation as a next-generation biomarker and diagnostic tool. Mol. Genet. Metab. 110 (1–2), 25–34.
Jafarian, I., Eskandari, M.R., Mashayekhi, V., Ahadpour, M., Hosseini, M.J., 2013. Toxicity of valproic acid in isolated rat liver mitochondria. Toxicol. Mech. Methods 23 (8), 617–623.
Jazwinski, S.M., 2013. The retrograde response: when mitochondrial quality control is not enough. Biochim. Biophys. Acta 1833 (2), 400–409.
Kaimal, V., Bardes, E.E., Tabar, S.C., Jegga, A.G., Aronow, B.J., 2010. ToppCluster: a multiple gene list feature analyzer for comparative enrichment clustering and network-based dissection of biological systems. Nucleic Acids Res. 38, W96–W102 (Web Server issue).
Kamburov, A., Pentchev, K., Galicka, H., Wierling, C., Lehrach, H., Herwig, R., 2011. ConsensusPathDB: toward a more complete picture of cell biology. Nucleic Acids Res. 39, D712–D717 (Database issue).
Khan, S.A., Leppäaho, E., Kaski, S., 2016. Bayesian multi-tensor factorization. Mach. Learn. 105 (2), 233–253.
Kiang, T.K., Ho, P.C., Anari, M.R., Tong, V., Abbott, F.S., Chang, T.K., 2006. Contribution of CYP2C9, CYP2A6, and CYP2B6 to valproic acid metabolism in hepatic microsomes from individuals with the CYP2C9*1/*1 genotype. Toxicol. Sci. 94 (2), 261–271.
Kotiadis, V.N., Duchen, M.R., Osellame, L.D., 2014. Mitochondrial quality control and communications with the nucleus are important in maintaining mitochondrial function and cell health. Biochim. Biophys. Acta 1840 (4), 1254–1265.
Kramer, O.H., Zhu, P., Ostendorff, H.P., Golebiewski, M., Tiefenbach, J., Peters, M.A., Brill, B., Groner, B., Bach, I., Heinzel, T., Gottlicher, M., 2003. The histone deacetylase inhibitor valproic acid selectively induces proteasomal degradation of HDAC2. EMBO J. 22 (13), 3411–3420.
Kulawiec, M., Safina, A., Desouki, M.M., Still, I., Matsui, S., Bakin, A., Singh, K.K., 2008. Tumorigenic transformation of human breast epithelial cells induced by mitochondrial DNA depletion. Cancer Biol. Ther. 7 (11), 1732–1743.
Kustatscher, G., Grabowski, P., Rappsilber, J., 2017. Pervasive coexpression of spatially proximal genes is buffered at the protein level. Mol. Syst. Biol. 13 (8), 937.
Kwiecinska, P., Wrobel, A., Tauboll, E., Gregoraszczuk, E.L., 2014. Valproic acid, but not levetiracetam, selectively decreases HDAC7 and HDAC2 expression in human ovarian cancer cells. Toxicol. Lett. 224 (2), 225–232.
Langmead, B., Trapnell, C., Pop, M., Salzberg, S.L., 2009. Ultrafast and memory-efficient alignment of short DNA sequences to the human genome. Genome Biol. 10 (3), R25.
Law, C.W., Chen, Y., Shi, W., Smyth, G.K., 2014. voom: precision weights unlock linear model analysis tools for RNA-seq read counts. Genome Biol. 15 (2), R29.
Le Novere, N., 2015. Quantitative and logic modelling of molecular and gene networks. Nat. Rev. Genet. 16 (3), 146–158.
Lehwald, N., Tao, G.Z., Jang, K.Y., Papandreou, I., Liu, B., Pysz, M.A., Willmann, J.K., Knoefel, W.T., Denko, N.C., Sylvester, K.G., 2012. beta-Catenin regulates hepatic mitochondrial function and energy balance in mice. Gastroenterology 143 (3), 754–764.
Li, B., Dewey, C.N., 2011. RSEM: accurate transcript quantification from RNA-Seq data with or without a reference genome. BMC Bioinf. 12, 323.
Liu, X.F., Jiang, H., Zhang, C.S., Yu, S.P., Wang, Z.Q., Su, H.L., 2012. Targeted drug regulation on methylation of p53-BAX mitochondrial apoptosis pathway affects the growth of cholangiocarcinoma cells. J. Int. Med. Res. 40 (1), 67–75.
Manev, H., Dzitoyeva, S., 2013. Progress in mitochondrial epigenetics. Biomol. Concepts 4 (4), 381–389.
Mo, Q., Wang, S., Seshan, V.E., Olshen, A.B., Schultz, N., Sander, C., Powers, R.S., Ladanyi, M., Shen, R., 2013. Pattern discovery and cancer gene identification in integrated cancer genomic data. Proc. Natl. Acad. Sci. U. S. A. 110 (11), 4245–4250.
Mukherjee, J., Mahato, B., Adhya, S., 2014. Vesicular transport of a ribonucleoprotein to mitochondria. Biol. Open 3 (11), 1083–1091.
Oliveros, J.C., 2007. VENNY. An Interactive Tool for Comparing Lists with Venn Diagrams.
Pessayre, D., Mansouri, A., Haouzi, D., Fromenty, B., 1999. Hepatotoxicity due to mitochondrial dysfunction. Cell Biol. Toxicol. 15 (6), 367–373.
Ponchaut, S., van Hoof, F., Veitch, K., 1992. In vitro effects of valproate and valproate metabolites on mitochondrial oxidations. Relevance of CoA sequestration to the observed inhibitions. Biochem. Pharmacol. 43 (11), 2435–2442.
Porreca, I., D'Angelo, F., Gentilcore, D., Carchia, E., Amoresano, A., Affuso, A., Ceccarelli, M., De Luca, P., Esposito, L., Guadagno, F.M., Mallardo, M., Nardone, A., Maccarone, S., Pane, F., Scarfo, M., Sordino, P., De Felice, M., Ambrosino, C., 2014. Cross-species toxicogenomic analyses and phenotypic anchoring in response to groundwater low-level pollution. BMC Genom. 15, 1067.
Rieswijk, L., Claessen, S.M., Bekers, O., van Herwijnen, M., Theunissen, D.H., Jennen, D.G., de Kok, T.M., Kleinjans, J.C., van Breda, S.G., 2016. Aflatoxin B1 induces persistent epigenomic effects in primary human hepatocytes associated with hepatocellular carcinoma. Toxicology 350–352, 31–39.
Ryan, M.T., Hoogenraad, N.J., 2007. Mitochondrial-nuclear communications. Annu. Rev. Biochem 76, 701–722.
Sarkar, S., Abujamra, A.L., Loew, J.E., Forman, L.W., Perrine, S.P., Faller, D.V., 2011. Histone deacetylase inhibitors reverse CpG methylation by regulating DNMT1 through ERK signaling. Anticancer Res. 31 (9), 2723–2732.
Schmidt, V.A., Chiariello, C.S., Capilla, E., Miller, F., Bahou, W.F., 2008. Development of hepatocellular carcinoma in Iqgap2-deficient mice is IQGAP1 dependent. Mol. Cell. Biol. 28 (5), 1489–1502.
Schumacher, J.D., Guo, G.L., 2015. Mechanistic review of drug-induced steatohepatitis. Toxicol. Appl. Pharmacol. 289 (1), 40–47.
Seibenhener, M.L., Du, Y., Diaz-Meco, M.T., Moscat, J., Wooten, M.C., Wooten, M.W., 2013. A role for sequestosome 1/p62 in mitochondrial dynamics, import and genome integrity. Biochim. Biophys. Acta 1833 (3), 452–459.
Silva, M.F., Ruiter, J.P., Jakobs, I.J.L.C., Duran, M., de Almeida, I.T., Wanders, R.J., 2001. Differential effect of valproate and its Delta2- and Delta4-unsaturated metabolites, on the beta-oxidation rate of long-chain and medium-chain fatty acids. Chem. Biol. Interact. 137 (3), 203–212.
Silva, M.F., Aires, C.C., Luis, P.B., Ruiter, J.P., I.J.L, Duran, M., Wanders, R.J., Tavares de Almeida, I., 2008. Valproic acid metabolism and its effects on mitochondrial fatty acid oxidation: a review. J. Inherit. Metab. Dis. 31 (2), 205–216.
Stekhoven, D.J., 2013. MissForest: Nonparametric Missing Value Imputation Using Random Forest.
Taiwo, O., Wilson, G.A., Morris, T., Seisenberger, S., Reik, W., Pearce, D., Beck, S., Butcher, L.M., 2012. Methylome analysis using MeDIP-seq with low DNA concentrations. Nat. Protoc. 7 (4), 617–636.
Tiwari, B., Sellamuthu, B., Ouarda, Y., Drogui, P., Tyagi, R.D., Buelna, G., 2017. Review on fate and mechanism of removal of pharmaceutical pollutants from wastewater using biological approach. Bioresour. Technol. 224, 1–12.
Tong, V., Teng, X.W., Chang, T.K., Abbott, F.S., 2005. Valproic acid II: effects on oxidative stress, mitochondrial membrane potential, and cytotoxicity in glutathione-depleted rat hepatocytes. Toxicol. Sci. 86 (2), 436–443.
van Breda, S.G.J., Claessen, S.M.H., van Herwijnen, M., Theunissen, D.H.J., Jennen, D.G.J., de Kok, T., Kleinjans, J.C.S., 2017. Integrative omics data analyses of repeated dose toxicity of valproic acid in vitro reveal new mechanisms of steatosis induction. Toxicology 393, 160–170.
Vinken, M., 2015. Adverse outcome pathways and drug-induced liver injury testing. Chem. Res. Toxicol. 28 (7), 1391–1397.
Vizcaino, J.A., Csordas, A., del-Toro, N., Dianes, J.A., Griss, J., Lavidas, I., Mayer, G., Perez-Riverol, Y., Reisinger, F., Ternent, T., Xu, Q.W., Wang, R., Hermjakob, H., 2016. 2016 update of the PRIDE database and its related tools. Nucleic Acids Res. 44 (D1), D447–D456.
Volonte, D., Liu, Z., Shiva, S., Galbiati, F., 2016. Caveolin-1 controls mitochondrial function through regulation of m-AAA mitochondrial protease. Aging (Albany N.Y.) 8 (10), 2355–2369.
Wisniewski, J.R., Zougman, A., Nagaraj, N., Mann, M., 2009. Universal sample preparation method for proteome analysis. Nat. Methods 6 (5), 359–362.
Wolters, J.E., van Herwijnen, M.H., Theunissen, D.H., Jennen, D.G., Van den Hof, W.F., de Kok, T.M., Schaap, F.G., van Breda, S.G., Kleinjans, J.C., 2016. Integrative −omics analysis in primary human hepatocytes unravels persistent mechanisms of cyclosporine A-induced cholestasis. Chem. Res. Toxicol. 29 (12), 2164–2174.
Wolters, J.E.J., van Breda, S.G.J., Caiment, F., Claessen, S.M., de Kok, T., Kleinjans, J.C.S., 2017. Nuclear and mitochondrial DNA methylation patterns induced by valproic acid in human hepatocytes. Chem. Res. Toxicol. 30 (10), 1847–1854.
Wu, D., Chen, X., Guo, D., Hong, Q., Fu, B., Ding, R., Yu, L., Hou, K., Feng, Z., Zhang, X., Wang, J., 2005. Knockdown of fibronectin induces mitochondria-dependent apoptosis in rat mesangial cells. J. Am. Soc. Nephrol. 16 (3), 646–657.
Yu, L., Liu, Y., Wu, Y., Liu, Q., Feng, J., Gu, X., Xiong, Y., Fan, Q., Ye, J., 2014. Smad3/Nox4-mediated mitochondrial dysfunction plays a crucial role in puromycin aminonucleoside-induced podocyte damage. Cell. Signal. 26 (12), 2979–2991.
Yu, D.M., Jung, S.H., An, H.T., Lee, S., Hong, J., Park, J.S., Lee, H., Bahn, M.S., Lee, H.C., Han, N.K., Ko, J., Lee, J.S., Ko, Y.G., 2017. Caveolin-1 deficiency induces premature senescence with mitochondrial dysfunction. Aging Cell 16 (Aug (4)), 773–784. http://dx.doi.org/10.1111/acel.12606. Epub 2017 May 17.